

# Fluorescence Photodiagnosics and Photobleaching Studies of Cancerous Lesions using Ratio Imaging and Spectroscopic Techniques

M.A. Scott<sup>1</sup>, C. Hopper<sup>1</sup>, A. Sahota<sup>1</sup>, R. Springett<sup>2</sup>, B.W. McIlroy<sup>1</sup>, S.G. Bown<sup>1</sup> and A.J. MacRobert<sup>1</sup>

<sup>1</sup>National Medical Laser Centre, Royal Free and University College Medical School, Institute of Surgical Studies, University College London, London, UK; <sup>2</sup>Department of Medical Physics and Bioengineering, University College London, UK

**Abstract.** Topical or systemic administration of 5-aminolaevulinic acid results in biosynthesis of the photosensitiser protoporphyrin IX (PpIX) with some selectivity for malignant lesions. Excitation near 400 nm excites both intrinsic green tissue autofluorescence and red fluorescence from PpIX which may be exploited for the optical diagnosis of malignant and premalignant disease. In this work the utility of a cooled 12-bit single chip charge-coupled device (CCD) colour camera was investigated for photodiagnostic fluorescence ratio imaging. The red to green fluorescence intensity ratios were calculated for each pixel in real-time and fluorescence ratio images were displayed typically at a rate of 2 frames/s. Laboratory tests of fluorescence ratio imaging showed good contrast enhancement between control tissues and tissue phantoms and those containing porphyrin photosensitisers. In preliminary clinical tests, a clear demarcation between neoplastic/cancerous lesions and adjacent normal tissue was demonstrated. The extent of PpIX photobleaching during photodynamic therapy was also investigated using fluorescence ratio imaging.

**Keywords:** 5-Aminolaevulinic acid; Fluorescence imaging; Optical biopsy; Photodiagnosics; Photodynamic therapy

## INTRODUCTION

In recent years, the need for new methods of early cancer detection has stimulated the rapid development of non-invasive optical diagnostic techniques [1]. Successful routine implementation would potentially increase cost effectiveness and clinical efficacy by reducing the number of conventional biopsies required. The recent availability of efficient, compact light sources and delivery systems has provided impetus for the application of fluorescence-based diagnostic techniques [2,3]. Moreover, the advent of highly sensitive charge coupled device (CCD) detection cameras and fast computer-controlled video capture boards have facilitated the acquisition

of high resolution maps of fluorescence phenomena in the temporal and frequency domains [4–6]. In principle, real-time fluorescence imaging may provide a more thorough and accurate assessment of the diseased tissue than can be attained by direct visual judgement.

The principles of fluorescence are well established [7] which in the case of porphyrins under excitation near 400 nm occurs when electrons are promoted into the higher lying  $S_2$  state followed by non-radiative relaxation to the radiative  $S_1$  state. Collagen, flavin adenine dinucleotide (FAD), nicotinamide adenine dinucleotide (reduced form, NADH) and elastin are well-known examples of intrinsic tissue fluorophores contributing to the broad autofluorescence spectrum observed in the blue and green spectral regions (450–580 nm) under blue or near-UV excitation in the range 300–450 nm [8]. In several studies, the intensity difference of this autofluorescence between normal and tumour tissue has been exploited for photodiagnosis, particularly for detection

---

Correspondence to: A. J. MacRobert, National Medical Laser Centre, Royal Free and University College Medical School, Institute of Surgical Studies, University College London, Charles Bell House, 67–73 Riding House St, London W1P 7LD, UK. Tel: 0171 380 9384, Fax: 0171 813 2828, e-mail: a.macrobert@ucl.ac.uk

of early lung tumours [9,10]. Various techniques have been established recently that combine multiple excitation and/or detection wavelengths with intensity ratioing to discriminate the tissue autofluorescence from the fluorescence of externally administered fluorescent markers, thereby improving tumour demarcation [4,11,12]. It has been widely observed that the autofluorescence intensity excited near 400 nm from normal tissue is higher than tumour in the range 450–550 nm, but lower in the range 600–700 nm and by taking the ratio of red intensity (600–700 nm) over the blue/green intensity (450–550 nm) the contrast between tumour and adjacent normal tissue is enhanced significantly [4]. Another important advantage of intensity ratioing is that it minimises the influence of variations in the excitation and detection geometry.

In recent years, the porphyrin precursor 5-aminolaevulinic acid (ALA) has proven useful as a fluorescent marker for tumours due to more biosynthesis of protoporphyrin IX (PpIX) in tumours than in the adjacent normal tissue in which the tumour arose after external ALA administration [13]. Although ALA is itself non-fluorescent, PpIX exhibits fluorescence in the red and near infrared (NIR) with maxima ca. 635 nm and 700 nm. The strong and relatively broad Soret band absorption ca. 410 nm provides a suitable excitation wavelength for both autofluorescence and PpIX fluorescence. These factors make ALA-induced PpIX attractive for fluorescence diagnostics in addition to its use for photodynamic therapy (PDT).

In PDT, light from an arc lamp or laser source at an appropriate wavelength and energy dosage leads to tissue necrosis following the external administration of a photosensitising drug. In the Type II PDT scheme, energy transfer from the long-lived triplet state of the photosensitiser to molecular oxygen results in the formation of cytotoxic singlet oxygen,  $^1\text{O}_2$  [14]. However, photobleaching of ALA-induced PpIX also occurs during PDT, most probably via a mechanism involving singlet oxygen, which limits the treatment efficacy [15–17]. In the case of photo-diagnosis, PpIX photobleaching can also be a limitation following excitation of the strong Soret band near 400 nm. Photobleaching may, however, serve as a useful means of monitoring PDT dosimetry [15] since the reduction in intensity of the PpIX fluorescence is primarily dependent on the irradiation fluence.

Superficial skin tumours are ideal for both fluorescence diagnostics and PDT since they are thin and easily accessible. Consequently, light delivery, photosensitiser administration and optical imaging are greatly simplified. Basal cell carcinomas (BCCs) are a very common form of sun-induced skin cancer which grow slowly and can cover areas as large as 1–4 cm<sup>2</sup>. Conventional methods for treating BCCs are surgical excision, cryosurgery and radiotherapy, which may involve significant patient discomfort and tissue scarring. Consequently methods for early detection and treatment of these lesions are desirable. PDT using topical ALA has proven to be effective in several studies [18–20]. Neoplastic oral tissues respond well to PDT treatment with minimal scarring and are ideally suited for fluorescence diagnostics due to the ease of accessibility and highly selective uptake of PpIX relative to normal tissues [12].

The primary aim of this paper is to describe the laboratory development and preliminary clinical applications of fluorescence ratio imaging to providing clear demarcation of tumour from normal tissue before, during and after PDT. Additionally, we outline both fluorescence imaging and spectroscopy techniques to monitor the photosensitiser photobleaching during PDT using ALA.

## MATERIALS AND METHODS

### Excitation Source and Light Delivery

The apparatus developed for acquiring fluorescence ratio and ‘white light’ images is shown schematically in Fig. 1. In dermatology clinics, Wood’s lamps are commonly used to excite and view skin conditions and incorporate a magnifying lens for viewing and a switch allowing either ultraviolet (UV-A) or white light output. In our clinic, a Wood’s lamp is used to excite the red photosensitiser fluorescence prior to PDT. The Wood’s lamp spectral output was noted to be dominated by a multitude of discrete lines characteristic of metal vapour discharges. Although strong fluorescence peaks were observed in the blue/violet region at 405 nm and 435 nm, concomitant contributions throughout the red and NIR region (650–800 nm) were observed. Although masked to the naked eye by the blue output, these extra emission bands render the Wood’s lamp less than ideal as an excitation source for

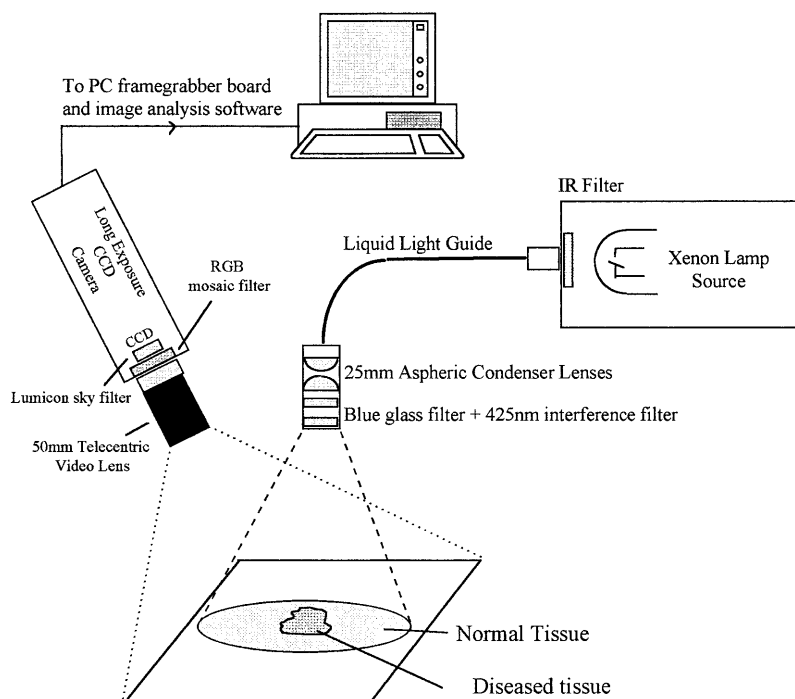


Fig. 1. Schematic diagram of the fluorescence ratio imaging apparatus.

quantitative fluorescence diagnostics. However, the lamp was applied during laboratory tests and for visual comparison of the lesion fluorescence with the captured CCD images in the clinic. As alternatives to laser sources, several other halide and xenon arc lamp sources for fluorescence excitation of PpIX were investigated. Of these, the Medisun-10 lamp (Medical Light Technologies Ltd, UK) incorporating a xenon arc source was employed due to the ease of portability and high optical power output.

The light delivery system consisted of a 8 mm diameter by 1 m long liquid light guide (Speirs Robertson Ltd, UK) with efficient blue and UV-A transmission in combination with two 18 mm aspheric lenses to provide a spatially uniform output beam at the tissue surface. Since xenon arc lamps emit over a broad spectral range ( $\lambda \sim 380\text{--}1250$  nm), efficient wavelength filtering of both the source and detected light is essential to obtain precise spectroscopic data. Various combinations of optical filters were fixed in front of the delivery system and the optimal configuration was found to be a fluorescence interference filter  $\lambda = 425 (\pm 17)$  nm (Corion Corp., MA, USA) combined with a bandpass filter transmitting wavelengths between 300 and 500 nm (BG12, Schott Glass, Germany). This wavelength output matched the strong PpIX Soret band absorption ca. 420 nm. The output power of the

blue light was kept at  $\sim 2$  mW/cm<sup>2</sup> to minimise photobleaching of the photosensitiser while maintaining adequate fluorescence intensities.

### Imaging Apparatus and Software

Fluorescence was imaged using a single chip CCD red/green/blue (RGB) colour camera (Sensicam, Personal Computer Optics, Germany) coupled to a 55 mm telecentric video lens (Computar Ltd, UK). The images were captured by a frame-grabber with an integrated analogue to digital converter (ADC) and analysed by a 233 MHz personal computer (Dell Computers Ltd, UK). Integration times of 0.5 s were typically employed.

There are several key advantages in using this camera for photodiagnostics.

1. The camera is Peltier cooled to a constant temperature of  $-17^\circ\text{C}$  to reduce the dark current to a low level ( $\sim 8$  electrons/pixel s). The sensitivity is therefore much improved over a standard video camera enabling lower doses of ALA to be used with lower excitation intensities: photobleaching of PpIX was consequently negligible during imaging. Electronic shuttering is employed and images ( $640 \times 480$  pixels) are integrated on-chip unlike video cameras where frame averaging is used which increases the overall read-out noise.

2. High read-out speed (12.5 Mhz) at up to 10 frames/s with 12-bit digitisation at 7 photoelectrons/count – standard video cameras only use 8-bit resolution. Double-correlation techniques are used to minimise read-out noise to  $\sim 3$  counts.
3. Integral to the camera is an RGB mosaic filter which provides the wavelength separation which is relatively good compared with other single-chip CCD cameras and comparable to 3-chip cameras. For ratio imaging only the red and green detection bands were used. However, there was inevitably some wavelength overlap between the spectral response curves in the green band (480–600 nm with peak response at 530 nm) and the red band (560–800 nm with peak response at 620 nm) [21]. In order to minimise this ‘crosstalk’ effect on the ratio imaging analysis we inserted a Na D-line rejection filter (Lumicon Corp., USA) in front of the mosaic filter. The filter is normally used for rejecting light pollution from sodium arc lines in astronomical applications and rejects wavelengths between 550 and 600 nm whilst efficiently transmitting the remaining green and red bands thereby removing the spectral overlap between the two bands. In addition, to minimise further the detection of scattered blue excitation light, a yellow longpass filter (GG475, Schott Glass, Germany) was placed in front of the CCD.

For the fluorescence ratio imaging, a dimensionless spatial variable ( $R$ ) was calculated according to the pixel coordinates ( $x,y$ ):

$$R(x,y) = \frac{I_{\text{red}}(600\text{--}800\text{ nm})}{I_{\text{green}}(480\text{--}550\text{ nm})} \quad (1)$$

Software was written to acquire and process the 12-bit red and green images and the ratio image map was displayed using a 12- to 8-bit data conversion algorithm [21]. Computation and display typically took 0.2 s. The wavelength bands are defined by the combination of the CCD mosaic filters and rejection filters. This ratio is largely independent of the tissue geometry and the incident light distribution and provides a quantitative measurement for correlation with subsequent histological assessment. The red band also includes an autofluorescence background, however, in this work the PpIX fluorescence around 635 nm was the dominant contribution. In order to record

the lesions in ambient white light, the integral Sensicam camera software was also used to acquire and store colour bitmaps. Further image analysis and conversion to pseudo-colour was achieved using the freely available image processing software packages Imagetool v2.0 (University of Texas Health Centre, USA) and ScionPC v. 2.0 (Scion Corp., USA).

### Fluorescence Microspectrofluorimetry

Fluorescence microscopy is an established technique for examining the location of ALA-induced PpIX fluorescence within tissues [22,23]. In this work fluorescence microscopy was combined with spectrometric probing of biopsies taken from a sensitised patient undergoing PDT treatment. Biopsy samples taken from the tumour were cut into 10  $\mu\text{m}$  cryosections, mounted on slides and placed on an inverted microscope stage (Olympus IMT-2, Japan). These were illuminated by a low power (1.8 mW) He-Ne laser operating at 543 nm (Uniphase, USA) to excite the fluorescence. The beam was confined to a spot of 100  $\mu\text{m}$  diameter using an aperture and was aligned within the tissue sample using a phase contrast image. The fluorescence was collected by a fiberoptic bundle placed at a trinocular port and dispersed by a Multispec 1/8 m focal length spectrograph (Oriel Instruments, USA) containing a 600 lines/mm diffraction grating blazed at 650 nm with a filter (RG 590, Schott long pass glass filter, Germany) to remove the green excitation light. The spectra were acquired by a slow scan CCD 600  $\times$  400 pixel detector (Mark II, Wright Instruments Ltd, UK) using a 10 s integration time. The spectral resolution of the system was 1 nm. No photobleaching effects were observed.

### Tissue Equivalent Optical Phantoms

For initial preclinical tests, two optical phantoms corresponding to the optical properties of human breast tissue were fabricated from epoxy containing scattering and absorbing compounds using a method similar to those used by Firbank and Delpy [24]. Since PpIX is photochemically and chemically labile the more stable and spectroscopically similar photosensitiser tetraphenylporphine (TPP) was used for this work. One of the phantoms contained TPP (at approx 10  $\mu\text{g/g}$  concentration)

while other acted as a control, thereby representing porphyrin-containing tissue and normal tissue, respectively.

### Human Skin Tissue Explants

Normal human skin explants were available from plastic surgical excisions. The tissues, weighing 70–100 mg, were floated in 2.5 ml of serum-free Dulbecco's DMEM/F-12 medium without phenol red, containing 50 IU/ml penicillin and 50  $\mu$ g/ml streptomycin. Incubations were performed at 37°C in an atmosphere of humidified air with 5% CO<sub>2</sub> in the dark in the presence of ALA and in the absence of ALA for control explants.

### Clinical Studies

For clinical evaluation, patients were selected who had easily accessible BCCs and oral dysplasia. In all cases the procedures were explained in detail and patient consent was given to undergo the non-invasive fluorescence diagnosis technique. At all times, the camera was secured on a tripod and placed perpendicular to the lesion of interest at a constant focal distance of 10 cm. The lens aperture was kept maximal and the camera exposure minimise to reduce movement artefacts in the images. Fluorescence imaging was always carried out in a dark room.

For PDT, a local anaesthetic was injected at the treatment site to reduce patient discomfort and the area illuminated uniformly by a broadband red LED array (Diomed Ltd, UK) with an incident fluence rate of 100 mW/cm<sup>2</sup> centred at  $\lambda=635$  nm. PDT treatment times were up to 1000 s per lesion corresponding to an incident fluence of 100 J/cm<sup>2</sup>. Grey scale and fluorescence ratio images of the lesions before and after PDT were acquired with ambient light and blue excitation light. Informed consent and ethical approval were obtained for these procedures.

## RESULTS

### Laboratory Tests of Fluorescence Ratio Imaging

To test the feasibility of the method prior to clinical application, images of the fluorescence intensities after blue light excitation from the

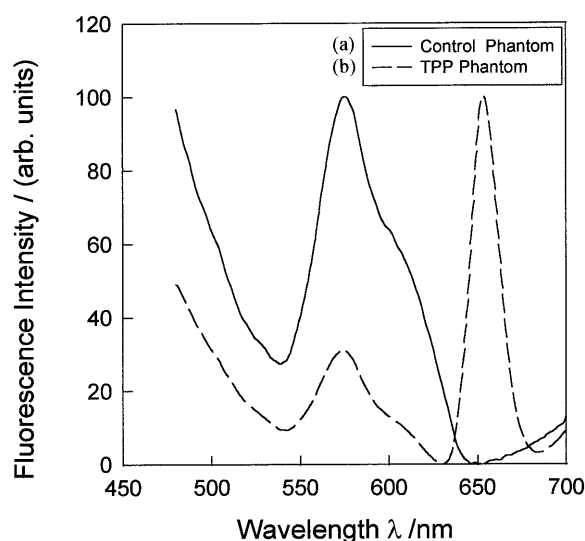


**Fig. 2.** Fluorescence spectra recorded by LS-50B spectrofluorimeter (10 nm slit width) in the wavelength range 470–700 nm after excitation at 410 nm of (a) control tissue phantom and (b) tissue phantom containing TPP(tetraphenylporphine) which was re-scaled to match the porphyrin peak (655 nm) with the maximum peak in the control.

tissue phantoms and human skin explants were acquired. When the tissue phantoms were placed adjacently and excited by the Wood's lamp, strong green fluorescence was visible from the control phantom whereas the TPP containing phantom exhibited an intense pink glow. The corresponding fluorescence spectra excited at 410 nm of the blocks recorded by a spectrofluorimeter (LS-50B, Perkin-Elmer) are shown in Fig. 2. Relatively little fluorescence was observed from the control beyond 650 nm whereas the phantom containing TPP fluoresced strongly near 650 nm corresponding to the TPP emission peak. Though not ideal, the relative fluorescence characteristics of this pair of phantoms were judged to be suitable for testing the ratio imaging routines. When viewed in grey scale image mode (Fig. 3a), both phantoms show comparable fluorescence intensities and only when the spectral red/green ratioing mode is used (Fig. 3b), can they be demarcated clearly. Indeed, the red/green intensity ratio is lowest at 0.5 where the emission from the intrinsic fluorophores in the control phantom are the sole contribution to the fluorescence intensity and maximal at 3 in the TPP phantom where red porphyrin fluorescence dominates. These phantoms were used subsequently for ratio calibration tests in the clinic.

Before the clinical studies we tested the system on *ex vivo* skin samples. Three skin

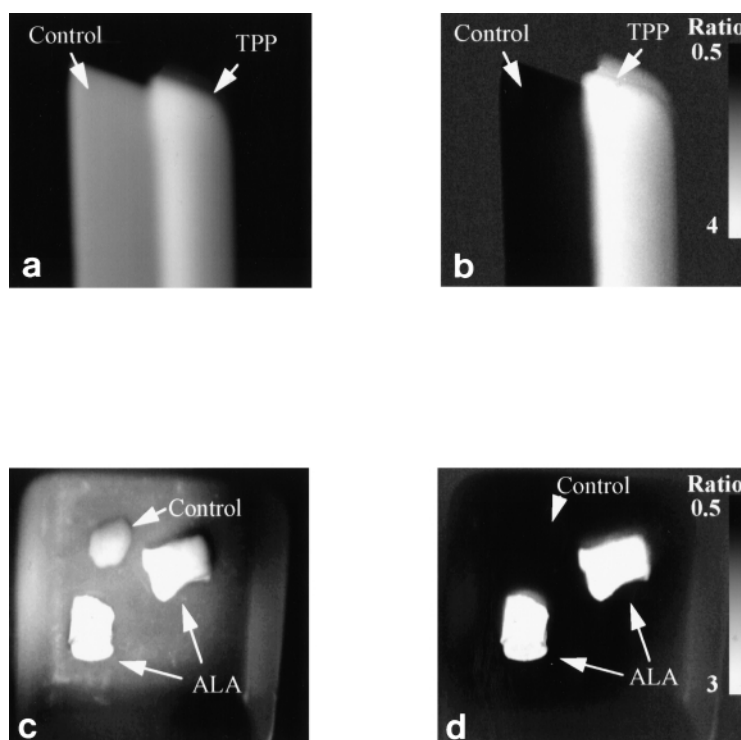


**Fig. 3.** (a) Grey scale CCD image after Wood's lamp excitation of TPP containing and control tissue phantoms. (b) Fluorescence intensity ratio image of (a) showing strong demarcation of the intrinsic green fluorescence from the red fluorescence in the TPP phantom. (c) Grey scale image after xenon lamp excitation at  $\lambda=420$  nm of two excised human tissue samples (incubated with ALA) and control sample (without ALA) as shown. (d) Fluorescence intensity ratio image of human skin samples as in (c) showing clear demarcation of the control sample from the ALA incubated tissues.

explants, two of which had been incubated for 6 h in 0.1 mM ALA solution to induce PpIX formation and one control sample, were imaged. The grey scale and ratio images under blue Xe lamp illumination are shown in Fig. 3(c) and (d), respectively. Clear demarcation of the tissue containing PpIX is shown in Fig. 3(d) with the R value peaking at a value of 3, which reflects the presence of the PpIX fluorescence in the 600–700 nm range as confirmed spectrometrically.

### Clinical Spectroscopic and Imaging Studies

#### *Fluorescence Spectroscopic Studies of Human BCC: Case Study 1*

Patient 1 was a male with a 3-year history of a non-healing crusted area behind the left ear which had been histologically diagnosed as a BCC. The central region of the lesion was thick and considered inappropriate for PDT but the lesion was so extensive that surgery alone would have necessitated a major resection and reconstructive procedure. Consequently, it was decided to undertake a com-

bination of surgery and PDT, with PDT to be applied to the extensive superficial disease and surgery for the thicker area of tumour. PDT was applied 4 h after systemic (oral, 60 mg/kg) ALA administration. Immediately before treatment a biopsy was taken from the tumour and subsequent biopsies were taken from the tumour surface at selected irradiation times and snap-frozen in liquid nitrogen-cooled isopentane. Cryosections 10  $\mu$ m thick were then prepared for micro-spectrofluorimetric studies. Using these samples it was possible to measure the fluorescence emission spectrum as a function of the incident fluence.

Figure 4 shows the fluorescence emission spectra from the tumour biopsies in the wavelength range 600–750 nm at increasing incident fluences of 0, 10, 20, and 50 J/cm<sup>2</sup>. The shape and wavelength peaks at ca. 635 nm and 705 nm agree well with the characteristic spectrum of PpIX and show a decrease in intensity with increasing irradiation time. However, it is notable that relatively little photoproduct signal ca. 670 nm is observed in this study.

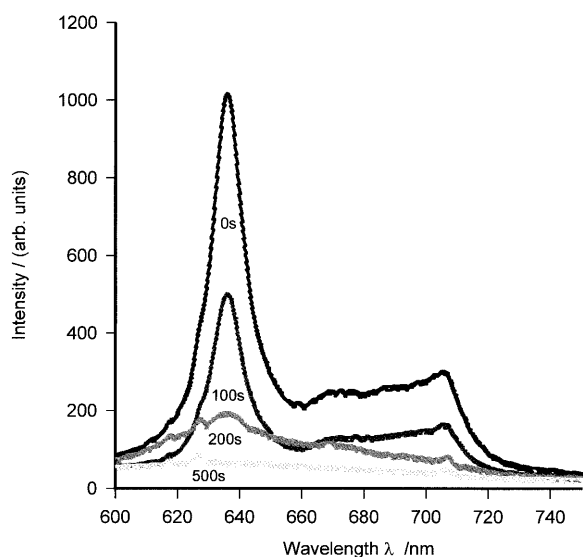


**Fig. 4.** Fluorescence spectra of BCC biopsies sampled at various PDT irradiation times as shown following oral ALA administration (60 mg/kg). The incident fluence rate was 100 mW/cm<sup>2</sup> and a 100 s irradiation corresponds to 10 J/cm<sup>2</sup>. Microspectrofluorimetry was performed on 10 μm cryosections with excitation at 543 nm supplied by a HeNe laser.

#### Fluorescence Ratio Imaging and PDT of BCC: Case Study 2

Patient 2 was a male who had numerous superficial and nodular BCC lesions of the back and chest areas some of which had been previously treated successfully in our clinic by PDT using ALA. One of the better demarcated lesions had a crusty, nodular appearance and was chosen for fluorescence study before, during and after PDT. The ALA powder was mixed with polyethylene glycol (Fluka, Switzerland, >98% purity) to form a 20% ALA, w/w, cream. The cream was liberally applied over and around the lesions and covered with a sterile, occlusive dressing as in other studies [19]. The cream was removed prior to fluorescence imaging.

The BCC lesion was imaged in colour with ambient background light prior to treatment as shown in Fig. 5(A). Only 1 h after topical ALA application, the lesion area exhibited a weak pink fluorescence which, when viewed through the Wood's lamp under UV excitation, became increasingly intense at up to 4 h after application. When excited with blue light from the xenon lamp, the corresponding fluorescence intensity ratio map was acquired and after pseudo-colour processing is shown in Fig. 5(B). Areas of high  $R$  values are represented by red whereas blue and green colours represent low ratios. The pink areas in the lesion correlate to  $I(\text{red,green})$  intensity val-

ues of (350,140) whereas the normal tissue areas have average  $I(\text{red,green})$  values of (20,100). Applying equation (1) yields the intensity ratio values  $R$  of 2.5 and 0.2 for the lesion and normal tissues, respectively. From the ratio of  $R$  values the overall contrast between tumour and normal is about a factor of 10. Of particular interest is the small area in Fig. 5(B) at the bottom right periphery of the lesion that exhibits a high fluorescence ratio which when viewed under normal white light does not appear to be BCC. Although a biopsy was not taken in this case to confirm the abnormality of the tissue, the fluorescence technique shows promise in demarcating the margin of tumour tissue more accurately than is available presently at the time of treatment.

After PDT for 1000 s (incident fluence of 100 J/cm<sup>2</sup>), the lesion showed only very weak PpIX fluorescence from the lesion area when viewed under the Wood's lamp. The fluorescence ratio image shown in Fig. 5(C) produces average  $I(\text{red,green})$  values of (110,105). The red intensity corresponding to PpIX has thus declined after PDT whereas the green autofluorescence was relatively unaffected.

#### Fluorescence Ratio Imaging in Oral Disease: Case Study 3

Patient 3 selected for fluorescence study had a history of oral cancer and severe dysplasia affecting the entire palatal mucosa. The diseased areas in the palate were treated using the photosensitiser *meta*-tetrahydroxyphenyl chlorin (mTHPC) with complete destruction of the tumour tissue [25]. Two years later, some moderate dysplasia had recurred and PDT using ALA was thought to be the most appropriate treatment modality. The extent and location of the disease was ideal for fluorescence diagnosis before and after PDT since the entire palate could easily be imaged and excited by the lamp light. ALA was administered orally at a total dosage of 60 mg/kg in three equal fractions over 2 h as described elsewhere [26] and imaging was carried out immediately before PDT treatment, 4 h after the initial ALA administration and after PDT.

The entire palate was imaged under ambient light as shown in Fig. 5(D). The dysplastic tissue manifests itself as white/pink regions while normal tissue is darker red. Blue excitation at ca. 420 nm was applied, and the intensity ratio image of the same area is shown in Fig. 5(E) after pseudo-colour conversion.

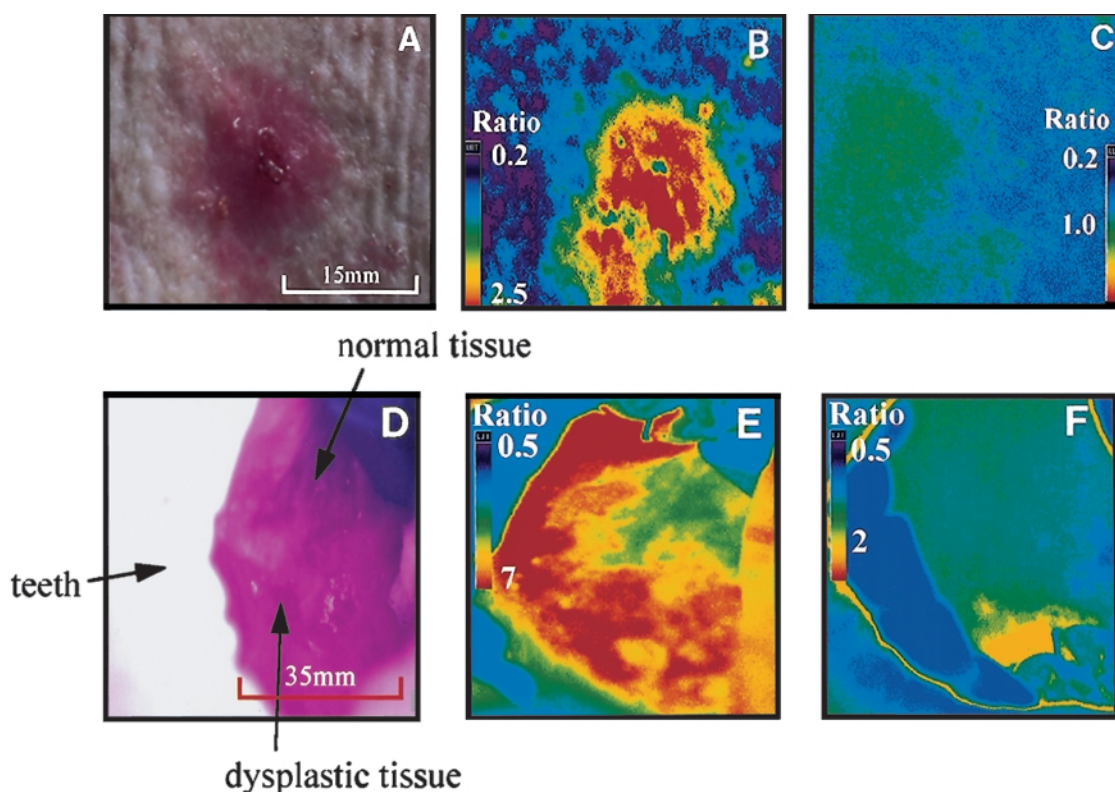


**Fig. 5.** (A) White light colour image of BCC lesion prior to ALA application. (B) Scaled pseudo-colour fluorescence ratio image of 5(A) after ALA application showing higher ratio in the tumour relative to surrounding normal skin. (C) Scaled pseudo-colour fluorescence ratio image after PDT. The centre of this image was displaced 10 mm to right of the tumour centre. (D) White light colour image of palate showing oral dysplasia sensitised with ALA-induced PpIX. (E) Scaled pseudocolour fluorescence ratio image of (D) showing enhanced enhanced ratio in the abnormal areas. (F) Scaled pseudocolour fluorescence ratio image after PDT showing reduced ratio values due to PpIX photobleaching.

The dysplastic areas were clearly characterised by strong red PpIX fluorescence with average  $I(\text{red,green})$  values of (1550,220) and, in the normal palate, lower average  $I(\text{red,green})$  values of (420,210) were observed. These led to  $R$  values of 7 and 2 for the dysplastic and normal tissues.

After the fluorescence study, PDT was applied over an area of  $\sim 10 \text{ cm}^2$  (incident fluence of  $100 \text{ J/cm}^2$ ) covering the diseased site and the fluorescence ratio image shown in Fig. 5(F) was obtained. The previously intense red fluorescence in the diseased areas had been much reduced, reflected by the average  $I(\text{red,green})$  values of (280,180) yielding a reduced  $R$  value of 2. The green autofluorescence intensity was relatively unaffected.

## DISCUSSION

Fluorescence intensity ratioing imaging provides a means of demarcating neoplastic and malignant tissues from normal due to the difference in both the spectral properties and

biosynthesis of PpIX after ALA administration. Under blue light excitation ca. 420 nm, tissue autofluorescence occurs maximally in the wavelength range 450–550 nm whereas broadband PpIX fluorescence is detected between 600 nm and 800 nm. The calculated intensity ratio of the red to green bands denoted here by  $R$  provides a means of correlating the relative tumour PpIX fluorescence. Preferential PpIX accumulation in abnormal tissues is due to a combination of factors: with systemic ALA administration, different activities of haem biosynthetic enzymes such as ferrochelatase are probably responsible [13,27]; whereas with topical administration, a higher penetration rate of ALA into tumour is an important factor. For photodiagnosis of oral tumours, topical administration of ALA would be more appropriate as found elsewhere [12], although it may still be necessary to use the systemic route for PDT treatment.

Photodiagnostic imaging using ALA-induced PpIX and other fluorophores has recently been reviewed [28,29] and our

approach is similar to other studies apart from differences in the ratio imaging technique. The imaging technique developed in the present study uses a sensitive cooled colour CCD camera incorporating a single-chip CCD, and intensity ratioing software which gives real-time, high quality image maps with clear demarcation between the tissue autofluorescence and the porphyrin fluorescence. The use of a cooled colour digital CCD enables low intensity quantitative fluorescence imaging to be carried out without the need for acquiring separate intensified CCD images of the porphyrin and autofluorescence spectral bands. Another approach benefiting from advances in CCD camera design and image processing software is the use of Fourier transform spectral imaging which has also been applied to ALA-induced PpIX diagnostics and, in the longer term, fluorescence lifetime imaging techniques may become more widely applied [6,28].

Prior to the clinical studies, the system was evaluated in the laboratory using epoxy phantoms and skin samples containing porphyrins. These samples yielded higher  $R$  values than the respective controls. In the clinical studies on BCC lesions and oral dysplasia,  $R$  values of 2.5 and 7 were obtained, whereas in the adjacent normal tissues lower  $R$  values were measured at 0.2 and 2, for BCC and oral dysplasia, respectively. The results on the BCC imaging are consistent with preferential synthesis of PpIX in the abnormal tissues observed elsewhere [28] although it is difficult to compare ratio imaging techniques quantitatively since the spectral widths and relative sensitivities of the imaging channels will vary between each system. In microspectrofluorimetric studies on a BCC lesion following systemic ALA administration, a large reduction in the integrated fluorescence intensity and a loss of the characteristic PpIX spectrum was observed in a series of biopsies taken over a total irradiation time of 500 s which corresponds to PpIX photobleaching/modification. In clinically applied PDT on the BCC and oral lesions, this photobleaching was manifested by a reduction in  $R$  values to 1.2 and 2, respectively, and little contrast was then evident between abnormal and normal tissue in the ratio images. The normal tissues maintained their  $R$  values indicating little light-induced photobleaching of the intrinsic tissue autofluorescence. In a recent study of the iontophoretic delivery of ALA in human skin tissues

[15], the degree of erythematous response as measured by the erythematous index was noted to depend strongly on the relative decrease in the PpIX fluorescence intensity induced by photobleaching. A strong erythematous PDT response was also visually noted for the BCC lesion image here and further studies examining the correlation between the PDT response in oral and cutaneous tumours and the change in the fluorescence ratio parameter  $R$  before and after treatment are planned. It is hoped that extending diagnostic imaging to monitoring of photobleaching may provide a means of determining a treatment end-point. A further refinement to the photobleaching analysis would be to confine the red imaging band to 610–650 nm so that any contribution from fluorescent photoproducts near 670 nm are minimised as far as possible. Although this study concentrated on the use of ALA as a photosensitiser precursor, the techniques are applicable to any of the photosensitisers presently in use for PDT, for example mTHPC (tetra *m*-hydroxyphenyl chlorin) and Photofrin<sup>®</sup>. In the near future, trials of endoscopic fluorescence diagnostic imaging will continue into other types of disease for example, lung carcinomas and gastrointestinal tumours. In addition, more detailed clinical studies of the correlation between fluorescence and conventional histological results are underway for the skin and oral lesions.

## ACKNOWLEDGEMENTS

One of us (BWM) is grateful to the EPSRC for the award of a research studentship. We would also like to thank Dr Adrianna Casas of the CIPYP, FCEYN, Buenos Aires, Argentina for help in preparing the human skin samples. MAS is indebted to the AICR for the award of a research fellowship.

## REFERENCES

1. Bigio IJ, Schneckenburger H, Slavik J, Svanberg K, Viallet PM (eds). SPIE Proceedings of conference on Progress in Biomedical Optics, Optical Biopsies and Microscope techniques II 1997;3197.
2. Andersson-Engels S, Elner A, Johansson J, Karlsson SE, Salford LG, Stromblad L et al. Clinical recording of laser-induced fluorescence spectra for evaluation of tumour demarcation feasibility in selected clinical specialities. *Lasers Med Sci* 1991;6:415–24.
3. Profio AE, Balchum OJ. Fluorescence diagnosis of cancer. *Adv Exp Med Biol* 1985;193:43–50.

4. Andersson-Engels S, af Klinteberg C, Svanberg K, Svanberg S. In vivo fluorescence imaging for tissue diagnostics. *Phys Med Biol* 1997;42:815–24.
5. Bigio IJ, Mourant JR. Ultraviolet and visible spectroscopies for tissue diagnostics: fluorescence spectroscopy and elastic-scattering spectroscopy. *Phys Med Biol* 1997;42:803–14.
6. Orenstein A, Kostenich G, Rothmann C, Barshack I, Mallik Z. Imaging of human skin lesions using multipixel fourier transform spectroscopy. *Lasers Med Sci* 1998;13:112–19.
7. Lakowicz JR. Principles of Fluorescence Spectroscopy. New York: Plenum Press, 1983.
8. Richards-Kortum R, Sevick-Muraca E. Quantitative optical spectroscopy for tissue diagnosis. *Annual Rev Phys Chem* 1996;47:555–606.
9. Hung J, Lam S, LeRiche JC, Palcic B. Autofluorescence of normal and malignant bronchial tissue. *Lasers Surg Med* 1991;11:99–105.
10. Lam S, MacAulay C, Palcic B. Detection and localization of early lung cancer by imaging techniques. *Chest* 1993;103:12S–14S.
11. Andersson-Engels S, Berg R, Svanberg K, Svanberg S. Multi-colour fluorescence imaging in connection with photodynamic therapy of  $\delta$ -amino levulinic acid (ALA) sensitised skin malignancies. *Bioimaging* 1997;42: 815–24.
12. Leunig A, Rick K, Stepp H, Gutmann RT, Alwin G, Baumgartner R et al. Fluorescence imaging and spectroscopy of 5-aminolevulinic acid induced protoporphyrin IX for the detection of neoplastic lesions in the oral cavity. *Am J Surg* 1996;172:674–677.
13. Kennedy JC, Marcus SL, Pottier RH. Photodynamic therapy (PDT) and photodiagnosis (PD) using endogenous photosensitisation induced by 5-aminolevulinic acid (ALA): mechanisms and clinical results. *J Clin Laser Med Surg* 1996;14(5):289–304.
14. Dougherty TJ, Gomer CJ, Henderson BW, Jori G, Kessel D, Korbek M et al. Photodynamic therapy. *J Natl Cancer Inst* 1998;90:889–905.
15. Rhodes LE, Tsoukas R, Rox Anderson R, Kollias N. Iontophoretic delivery of ALA provides a quantitative model for ALA pharmacokinetics and PpIX phototoxicity in human skin. *J Invest Dermatol* 1997;1:87–91.
16. Van der Veen N, De Bruijn HS, Star WM. Photobleaching during and re-appearance after photodynamic therapy of topical ALA-induced fluorescence in UVB-treated mouse skin. *Int J Cancer* 1997;72:110–18.
17. Wilson BC, Patterson MS, Lilge L. Implicit and explicit dosimetry in photodynamic therapy: a new paradigm. *Lasers Med Sci* 1997;12:182–99.
18. Alvanopoulos K, Antoniou C, Melpo P, Vareltzidis A, Katsambas A. Photodynamic therapy of superficial basal cell carcinomas using exogenous 5-aminolevulinic acid and 514-nm light. *J Eur Acad Dermatol Venereol* 1997;9:134–6.
19. Morton CA, MacKie Whitehurst C, Moore JV, McColl JH. Photodynamic therapy for basal cell carcinoma: effect of tumor thickness and duration of photosensitizer application on response. *Arch Dermatol* 1998;138:248–9.
20. Cairnduff F, Stringer MR, Hudson EJ, Ash DV, Brown SB. Superficial photodynamic therapy with topical 5-aminolaevulinic acid for superficial primary and secondary skin cancer. *Br J Cancer* 1994;69:605–8.
21. Sencicam Operating manual. PCO Computer Optics GmbH Germany, 1996.
22. Chang SC, Buonaccorsi G, MacRobert AJ, Bown SG. 5-Aminolevulinic acid (ALA)-induced protoporphyrin IX fluorescence and photodynamic effects in the rat bladder: An in vivo study comparing oral and intravesical ALA administration. *Lasers Surg Med* 1997;20:254–64.
23. Wilson BC, Olivo M, Singh G. Subcellular localization of Photofrin<sup>®</sup> and aminolevulinic acid and photodynamic cross-resistance in vitro in radiation-induced fibrosarcoma cells sensitive or resistant to photofrin-mediated photodynamic therapy. *Photochem Photobiol B* 1997;65:166–76.
24. Firbank M, Delpy DT. A phantom for the testing and calibration of near-infrared spectrometers. *Phys Med Biol* 1994;39:1509–13.
25. Fan KFM, Hopper C, Speight PM, Buonaccorsi GA, Bown SG. Photodynamic therapy using mTHPC for malignant disease the oral cavity. *Int J Cancer* 1997;73:25–32.
26. Fan K, Hopper C, Speight PM, Buonaccorsi G, MacRobert AJ, Bown SG. Photodynamic therapy using 5-aminolaevulinic acid for pre-malignant lesions of the oral cavity. *Cancer* 1996;78:1374–83.
27. van Hillegersberg R, van der Berg JW, Kort WJ, Terpstra OT, Wilson JHP. Selective accumulation of endogeneously produced porphyrins in a liver metastasis model in rats. *Gastroenterology* 1992;103:647–51.
28. Wagnieres GA, Star W, Wilson BC. In vivo fluorescence spectroscopy and imaging for oncological applications. *Photochem Photobiol* 1998;68:603–32.
29. Baumgartner R, Stepp H. Photodynamic diagnosis using 5-aminolaevulinic acid for minimally invasive treatment of cancer. *Min Invas Ther Allied Technol* 1998;7:495–510.